Journal of Alloys and Compounds 506 (2010) 862–867

Contents lists available at ScienceDirect

Journal of Alloys and Compounds

journal homepage: www.elsevier.com/locate/jallcom

Preparation and properties of $(1-x)BiFeO_3$–$xBaTiO_3$ multiferroic ceramics

Felicia Prihor Gheorghiu [a,*], Adelina Ianculescu [b], Petronel Postolache [a], Nicoleta Lupu [c], Marius Dobromir [a], Dumitru Luca [a], Liliana Mitoseriu [a]

[a] Department of Solid State and Theoretical Physics, Al. I. Cuza University, Bv. Carol I no. 11, Iasi 700506, Romania
[b] Polytechnics University of Bucharest, 1-7 Gh. Polizu, P.O. Box 12-134, 011061 Bucharest, Romania
[c] National Institute of Research and Development for Technical Physics, Iasi 700050, Romania

ARTICLE INFO

Article history:
Received 17 April 2010
Received in revised form 9 July 2010
Accepted 12 July 2010
Available online 23 July 2010

Keywords:
Multiferroic
$BiFeO_3$-based solid solutions
Magnetism

ABSTRACT

Solid solutions of $(1-x)BiFeO_3$–$xBaTiO_3$ ($0 \le x \le 0.30$) have been prepared by a two-step solid state reaction. By comparison with other reported methods, a higher electrical homogeneity of the ceramic bodies resulted in better dielectric properties, with a single-component impedance plot, small losses and permittivities below 240. The maximum magnetization is observed for $x = 0.05$, which might represent the proper range of compositions for multiferroism at room temperature. In order to better understand the composition-dependent magnetic properties in correlation with the expected Fe^{2+}/Fe^{3+} ratio fluctuations in the solid solutions, a detailed X-ray Photoelectron Spectroscopy (XPS) analyses were performed on the surfaces and on the fractured sintered bodies.

1. Introduction

$BiFeO_3$ is one of the few single-phase magnetoelectric multiferroics at room temperature and one of the most studied and controversial systems in the last years [1–3]. $BiFeO_3$ shows a distorted perovskite structure with rhombohedral symmetry (space group $R3c$ with lattice parameters: $a = 3.958$ Å, and $\alpha = 89.30°$), high ferroelectric Curie temperature ($T_C = 830$ °C) which was expected to be accompanied by a large spontaneous polarization (~100 μC/cm^2). From the magnetic point of view, it has an antiferromagnetic order (Néel temperature $T_N = 370$ °C, magnetic Curie temperature ~600 °C) and shows a weak ferro/ferrimagnetic characteristic in some temperature ranges [4–8]. The Fe magnetic moments are coupled ferromagnetically within the pseudocubic (1 1 1) planes and antiferromagnetically between adjacent planes (so-called G-type or cycloidal antiferromagnetic order). Although only small polarizations (below ~10 μC/cm^2) have been generally reported in its single crystal form [9], very high remanent polarizations above 100 μC/cm^2 were instead found in films with both rhombohedral and tetragonal symmetry [8,10,11]. Recently, similar high polarizations were also found in single-crystals [12]; however still poor ferroelectric and dielectric properties are typical for $BiFeO_3$ ceramics, due to the low resistivity at room temperature [13]. One of the reasons for this behavior was considered the difficulty to obtain pure $BiFeO_3$ ceramics, since the kinetics of phase formation in the Bi_2O_3–Fe_2O_3 system can easily lead to the appearance of impurities along with the perovskite major phase. The formation of secondary phases like $Bi_2Fe_4O_9$, $Bi_{25}FeO_{40}$ or $Bi_{46}Fe_2O_{72}$ was reported in ceramics [14,15], even after adopting some special strategies suggested by Achenbach and Sosnowska et al. [16,17]. Pure $BiFeO_3$ ceramics were eventually obtained more recently, by using sol–gel processing followed by rapid sintering [18], self-combustion [19], by other wet chemistry routes [20] and even by solid-state method, using a two-step process [21]. However, their dielectric and ferroelectric properties are still far from that reported for films, being generally characterized by high leakage, small permittivity, high dielectric losses and multiple thermally activated relaxations in kHz range.

To prevent the formation of secondary phases in ceramics and also to overcome the limit of poor dielectric characteristics, in recent studies the method of forming solid solutions of $BiFeO_3$ with other ABO_3 perovskites, such as $BaTiO_3$ or $PbTiO_3$ [15,21–24] or doping in A or B positions was largely adopted [25–28]. Some of these compounds show indeed better dielectric properties with higher polarization and almost saturated $P(E)$ loops, but a large dispersion of their functional characteristics and still controversial explanations for their functional properties were given (including the magnetic ones).

Recently $(1-x)BiFeO_3$–$xBaTiO_3$ ceramics ($x = 0$, 0.05, 0.10, 0.15, 0.20. 0.25 and 0.30) with good purity and homogeneity were prepared by mixed oxides method following a two-step sintering [21]. This method allowed not only to obtain a higher purity of the perovskite phase even for $x = 0$, but also to get rather good dielectric properties at room temperatures, with permittivities of

* Corresponding author.
E-mail address: felicia_prihor@stoner.phys.uaic.ro (F.P. Gheorghiu).

0925-8388/$ – see front matter © 2010 Elsevier B.V. All rights reserved.
doi:10.1016/j.jallcom.2010.07.098

around (180–250) and losses below 3% at frequencies in the range of (1–10^6) Hz [29]. A detailed study of the functional properties of $(1-x)BiFeO_3$–$xBaTiO_3$ solid solutions was not reported.

The aim of the present work was to study the dielectric and magnetic properties of the $(1-x)BiFeO_3$–$xBaTiO_3$ ceramics with compositions of $0 \le x \le 0.30$. The solid solutions prepared by two-step sintering method show an improvement of the dielectric characteristics, by comparison with literature data. A composition and temperature-dependent magnetic order was found. The origin of the observed magnetic properties is also discussed.

2. Experimental

The $(1-x)BiFeO_3$–$xBaTiO_3$ ($0 \le x \le 0.30$) ceramics were prepared by a two-step solid-state sintering from high purity oxides and carbonates: Bi_2O_3 (99.999%; Sigma–Aldrich), Fe_2O_3 (99.98%, Sigma–Aldrich), TiO_2 (99.99%; Sigma–Aldrich) and $BaCO_3$ (99.98%; Sigma–Aldrich). It was realised a pre-sintering at 650 °C/2 h followed by sintering at 800 °C/1 h and slow cooling, as described in detail in the Ref. [21].

The phase composition and crystal structure after sintering were checked with a SHIMADZU XRD 6000 diffractometer with Ni-filtered Cu Kα radiation (λ = 1.5418 Å), 0.02° scan step and 1 s/step counting time. A HITACHI S2600N scanning electron microscope SEM coupled with EDX was used to analyze the ceramics microstructure.

The dielectric measurements at room temperature in the frequency range 20 Hz–2 MHz, were performed by using an impedance bridge Agilent E4980A Precision LCR Meter. The magnetic properties in the range of temperatures (5–300) K under fields of (0–60) kOe were determined with a superconducting quantum interferometric device SQUID magnetometer (Quantum Design) and above room temperature with a MicroMag™ VSM model 3900 Vibrating Sample Magnetometer (Princeton Measurements Co.) under magnetic fields in the range of (0–20) kOe. The thermomagnetic data for pure $BiFeO_3$ ceramic were recorded to a field heating/field cooling cycle (FH/FC) under a dc field H = 10 kOe with a heating/cooling rate of 10 K/min. The magnetic properties for the $(1-x)BiFeO_3$–$xBaTiO_3$ ceramics were determined in the range of temperatures (300–1000) K under heating/cooling field H = 1 T with a LakeShore VSM 7410 magnetometer. The XPS spectra were measured using a PHI 5000 VersaProbe XPS instrument. The pressure in the chamber was of 2×10^{-6} Pa and the conditions used for all of the survey scans were: energy range of 130–750 eV, 117.4 eV pass energy, 0.5 eV step size and time/step of 20 ms. XPS spectra were recorded by using a PHI Summitt XPS software and the data were analysed with MultiPak Spectrum software. All the spectra were calibrated using the C 1s peak with a fixed value of 284.5 eV.

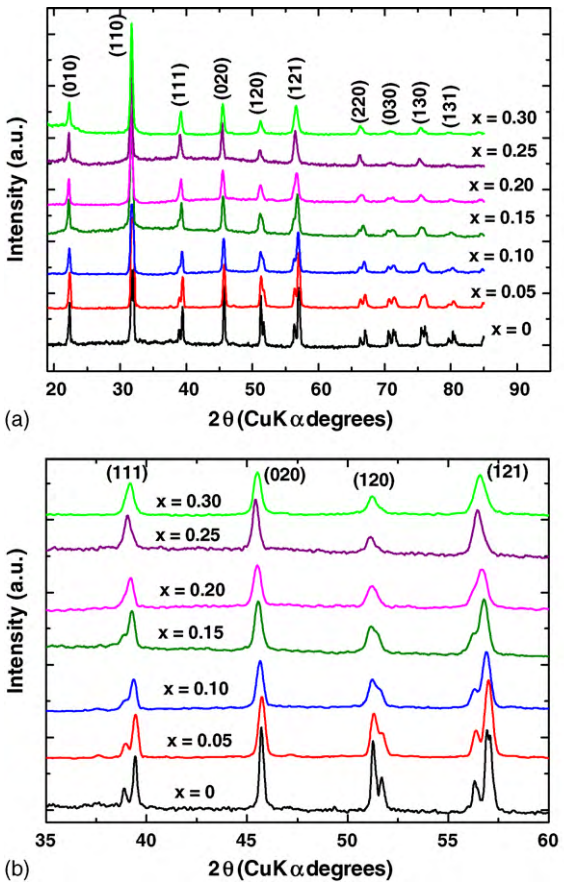

Fig. 1. (a) Room temperature X-ray diffraction patterns of the $(1-x)BiFeO_3$–$xBaTiO_3$ ceramics pre-sintered at 650 °C/2 h, sintered at 800 °C/1 h and slow cooled; (b) detailed XRD pattern showing the cancellation of splitting for (1 1 1), (1 2 0) and (1 2 1) peaks, when increasing x.

3. Results and discussions

3.1. Phase purity and microstructures

The room temperature XRD patterns (Fig. 1(a)) show perovskite single-phase, in the limit of XRD accuracy for all the investigated compositions after pre-sintering at 650 °C/2 h followed by sintering at 800 °C/1 h and slow cooling. For all investigated ceramics, perovskite structure of rhombohedral *R3c* symmetry was identified, with a gradual attenuation of the rhombohedral distortion with the increase of $BaTiO_3$ content. This tendency to a gradual change towards a cubic symmetry with the $BaTiO_3$ addition is proved by the cancellation of the splitting of the XRD (1 1 0), (1 1 1), (1 2 0), (1 2 1), (2 2 0), (0 3 0) maxima specific to pure $BiFeO_3$ ($2\theta \approx 31.5°$, 39°, 51°, 57°, 66°, 70°, 75°), as observed in the detailed representation from Fig. 1(b). The expansion of the lattice parameters with the increase of the $BaTiO_3$ content in $(1-x)BiFeO_3$–$xBaTiO_3$ system was also pointed out earlier [29]

SEM investigation performed on the surface of the $BiFeO_3$ pellet sintered at 800 °C/1 h pointed out a heterogeneous microstructure with bimodal grain size distribution, consisting from large grains with equivalent average size of ~25 μm and small grains of 3–4 μm (Fig. 2(a)). The micrograph of the ceramic sample with x = 0.15 (Fig. 2(b)) shows the dramatic influence of the $BaTiO_3$ on the microstructural features. One can observe the inhibiting effect of barium titanate on the grain growth process. Further increase of $BaTiO_3$ content to x = 0.30 (Fig. 2(c)) seems not to determine a further drop in the average grain size of the corresponding ceramic. Consequently, in both cases a rather monomodal grain size distribution and relative homogenous microstructures, consisting of a certain amount of intergranular porosity and finer (submicron) grains were observed [21,29].

3.2. Complex impedance characterisation

The dielectric properties of $(1-x)BiFeO_3$–$xBaTiO_3$ ceramics were investigated in detail in the Ref. [29]. They showed values of permittivity of (180, 240) and low losses at room temperatures in the whole range of composition ($\tan\delta$ < 3% for pure $BiFeO_3$ and $\tan\delta$ < 1.5% for all the solid solutions). In the literature, values of the room temperature permittivity below 100 and losses either $\tan\delta$ < 10% or even $\tan\delta$ > 1 were reported for $BiFeO_3$-based ceramics [13,15,18,22,23,26]. At room temperature, the complex impedance plots show a single-component irrespective of composition (x), as presented in Fig. 3. This demonstrates that the two-steps method of preparation lead to a better electrical homogeneity within the ceramic bodies by comparison with the $(1-x)BiFeO_3$–$xBaTiO_3$ ceramics previously prepared by a single sintering step, for which multiple semicircles in the impedance spectra were reported [21]. The homogeneity of a polycrystalline ceramic from electrical point of view is expressed by similar values of capacitance C and loss resistance R everywhere in the ceramic sample body. The ceramic is thus described by a unique (R, C) combination in the entire volume and this give rise to a complex impedance characteristic with only one semicircle plot [30]. Thus, the dielectric characteristics at room temperature of the ceramics prepared by the two-step sintering method were clearly improved.

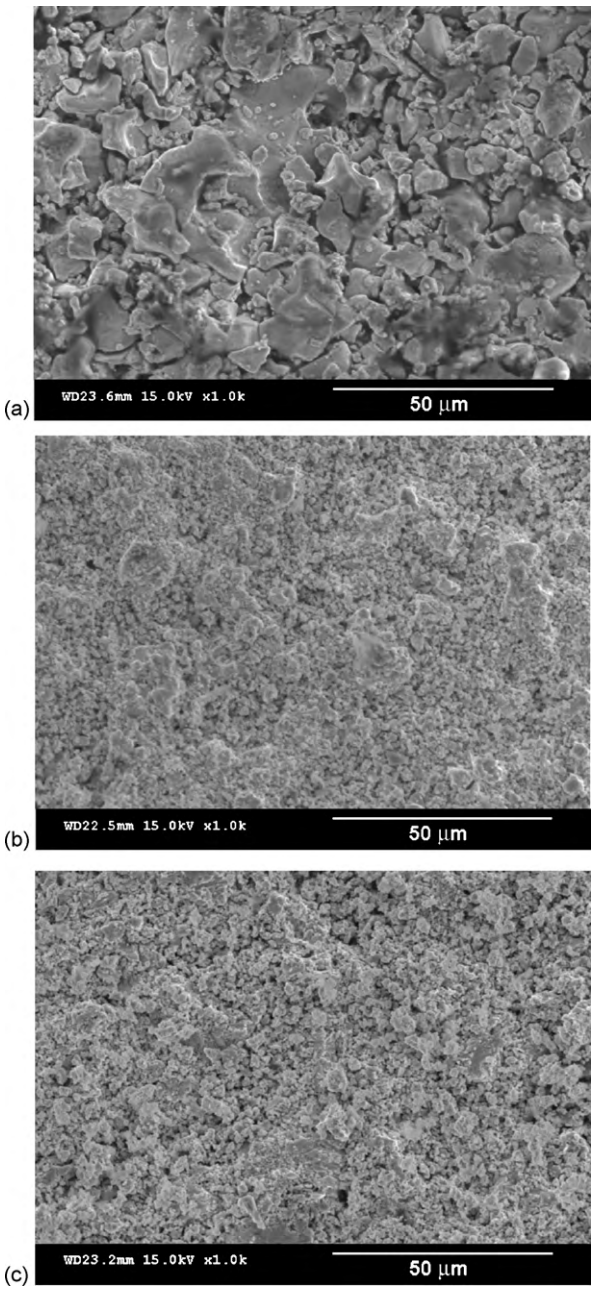

Fig. 2. Surface SEM images of the $(1-x)BiFeO_3$–$xBaTiO_3$ ceramics: (a) $x=0$, (b) $x=0.15$ and (c) $x=0.30$.

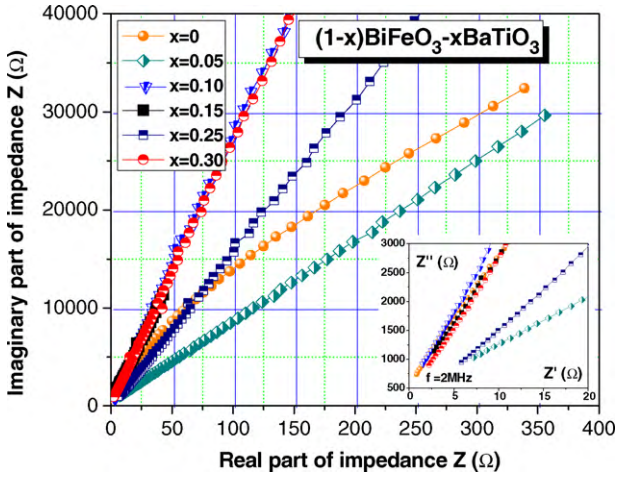

Fig. 3. Complex impedance diagram of the $(1-x)BiFeO_3$-$xBaTiO_3$ ceramics in the range of 1 Hz–2 MHz. (Inset) High frequency region. One single impedance component is observed.

3.3. Magnetic properties

3.3.1. $BiFeO_3$ ceramics

The properties of the as-sintered $BiFeO_3$ ceramics were firstly investigated. In the low-temperature range, a linear non-saturated dependence $M(H)$ as result of the cycloidal canted antiferromagnetic behavior was observed with a space modulated spin structure expected for this system [5,15,18,19]. A very small nonlinearity at 5 K, as due most probably to a field-induced weak ferromagnetism was also revealed (Fig. 4(a)). After this experiment, the same $BiFeO_3$ ceramic sample was subjected to a thermomagnetic measurements under a FH/FC cycle in the temperature range of (300–1000) K under a magnetic field $H=10$ kOe. The recorded magnetization *vs.* temperature data $M(T)$ obtained for the $BiFeO_3$ ceramic during the FH/FC cycle (Fig. 4(b)) confirm the expected behavior reported in various $BiFeO_3$-based systems [31,32]. The magnetization decreases with temperature, showing a small anomaly at the Neél temperature $T_N \sim 643$ K on heating and by the cancellation of the magnetization at the magnetic Curie temperature (~830–890 K). A small thermal hysteresis of ~60 K at the Curie temperature was noticed, that is typical for the first-order phase transitions. A radical change of the magnetic order in $BiFeO_3$ ceramics resulted after the FH/FC cycle under the magnetic field of $H=10$ kOe: the room-temperature magnetization becomes around 6 times higher than before performing the FH/FC experiment (Fig. 4(b)). The $M(H)$ loops at room temperature confirmed the modification of the magnetic order: a ferrimagnetic slim and well-saturated $M(H)$ dependence is obtained at room temperature, as presented in Fig. 4(c). The field-induced magnetization increases from 0.1–0.15 emu/g in the as-sintered ceramic to above 25 emu/g (after the thermomagnetic treatment), for a given value of the applied field ($H=20$ kOe). This magnetic behavior is very stable in time.

XRD analysis performed in order to detect possible phase modifications induced by the thermal treatment under the magnetic field FC indicated the absence of any secondary phase or structural modifications (changes of the unit cell parameters), in the limit of accuracy of the XRD experiments.

One possible explanation for the observed behavior may be related to the fact that spinoidal antiferromagnetism of the as-prepared $BiFeO_3$ was easily turned into a ferrimagnetic state after the thermomagnetic FH/FC sequence, whereas much higher fields above 280 kOe at $T=10$–180 K were reported in the literature to induce changes of the spinoidal antiferromagnetism into a regular spin order in $BiFeO_3$ [33]. In our case a smaller field is necessary for the spin re-orientation, due to the combined effect of high temperature and magnetic field application during the FC process.

Another possibility to explain the observed phenomena might be related to the existence of secondary phases. As indicated in the literature, several phases of different structures and compositions might coexist in the Bi–Fe–O system. Their presence even in small amounts can substantially affect the electrical and magnetic properties of the overall material. While α-Fe_2O_3 is a canted antiferromagnetic material with a weak magnetization of 0.4 emu/cm^3 at room temperature [34,35], bulk γ-Fe_2O_3 displays in contrast, magnetization up to ~400 emu/cm^3 at room temperature [36]. Co-existence of $BiFeO_3$ with small amounts of α,γ-Fe_2O_3 phases in films grown by pulsed laser deposition under various oxygen pressure was reported [37]. The presence of small amounts of maghemite γ-Fe_2O_3 was also evidenced in $BiFeO_3$ films grown

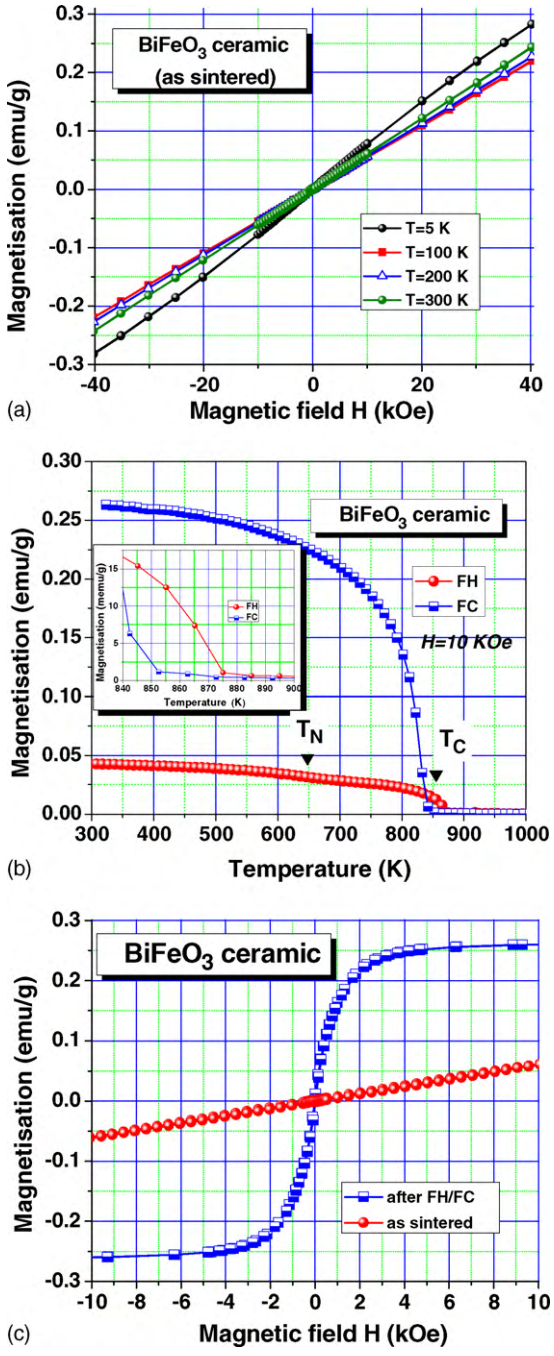

Fig. 4. Magnetic characteristics of the $BiFeO_3$ ceramics: (a) $M(H)$ dependence of as-sintered $BiFeO_3$ ceramics at $T = 5$, 100, 200, 300 K; (b) Thermomagnetic data $M(T)$ of $BiFeO_3$ ceramics on a FH/FC cycle (FH: field heating, FC: field cooling, $H = 10$ kOe). (Inset) Thermal hysteresis; (c) $M(H)$ loops at $T = 300$ K, after the thermomagnetic cycle (FH/FC).

in non-optimal conditions and this secondary phase was considered as being the main source of high magnetization observed in such films [38]. Detailed Raman investigations performed in $BiFeO_3$ films prepared by sol–gel show the formation of magnetite spinel phase Fe_3O_4 after the application of dc voltage of ~700 kV/cm for a few seconds and the absence of any α,γ-Fe_2O_3 phases [39]. It seems therefore possible that even in the case of the present $BiFeO_3$ ceramics, the conjugated effect of high temperature and magnetic field applied during cooling (FC) could give rise to: (i) small amounts of secondary phases with higher magnetization (e.g. γ-Fe_2O_3, Fe_3O_4, etc.) and/or (ii) field-induced

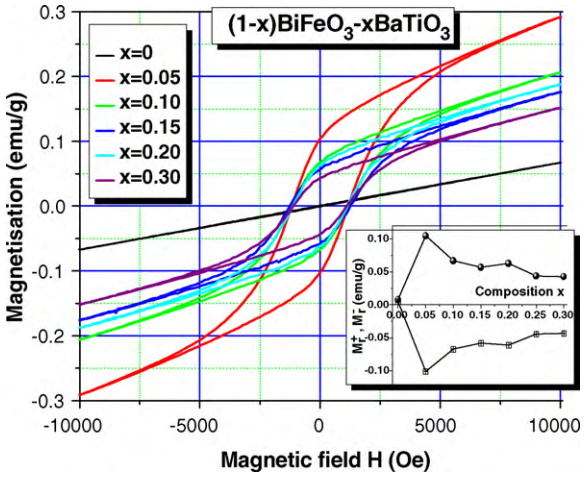

Fig. 5. Magnetic hysteresis loops for the solid solutions $(1-x)BiFeO_3$–$xBaTiO_3$ ($0 \le x \le 0.30$) at $T = 300$ K. (Inset) Remanent magnetization *vs.* $BaTiO_3$ composition.

spin re-orientation causing a transition from canted antiferromagnetism to ferri/ferromagnetic order. Both possibilities caused a higher room-temperature magnetization after the thermomagnetic cycle, as observed in our experiments. The co-existence of $BiFeO_3$ with other Fe–O magnetic phases and the low stability of the magnetic order when subjected to magnetic, electric fields, pressure and thermal cycles might also explain the large scattering of the magnetic properties reported for $BiFeO_3$-based compounds in the literature [5,15,18,19].

3.3.2. $(1-x)BiFeO_3$–$xBaTiO_3$ solid solutions

The magnetic properties of the $(1-x)BiFeO_3$–$xBaTiO_3$ ceramics show very interesting features. The magnetic hysteresis loops for the as-prepared $(1-x)$ $BiFeO_3$–$xBaTiO_3$ solid solutions at room temperature (Fig. 5) show that the antiferromagnetic behavior of $BiFeO_3$ (linear $M(H)$ dependence) is turned into a weak ferromagnetic state by addition of $BaTiO_3$. The highest magnetization, coercive field and $M(H)$ loop area were found for the composition $x = 0.05$. A transition from the spinoidal structure of pure $BiFeO_3$ to the homogeneous ferromagnetic state in $BiFeO_3$-based compounds induced by doping with non-magnetic ions was reported in the Ref. [26] and it was explained by changes in the bond angle of Fe–O–Fe caused by the distortion created by Ti and Ba co-doping, beside the changes of the statistical distribution of Fe^{3+}/Fe^{2+} as result of the charge compensation. An increasing magnetization was also reported by Itoh et al. [40] for small amounts of $BaTiO_3$ addition in $BiFeO_3$–$BaTiO_3$ solid solutions.

Thermomagnetic experiments of $(1-x)BiFeO_3$–$xBaTiO_3$ ceramics were performed for temperatures in the range (300–1000)K according to a FC/FH sequence under a magnetic field $H = 1$ T and the results are presented in Fig. 6(a and b). The variation of their magnetization against the temperature $M(T)$ shows indeed the presence of a temperature-dependent magnetic order, with magnetic moments (under the excitation field $H = 1$ T) which monotonously decrease with the temperature increase. The FH process (Fig. 6(a)) is characterized by two evident anomalies. The first one is indicated by a maximum around ~860 K, which seems to be independent on $BaTiO_3$ additions and is related to the magnetic Curie temperature of $BiFeO_3$ [4–8]. Another anomaly is around 631 K for $x = 0.05$ and reduces with increasing x, being impossible to be detected for $x \ge 0.20$ in the $M(T)$ dependence. However, the derivative dM/dT shows that this anomaly is still present and its corresponding temperature reduces down to ~534 K for $x = 0.30$ when increasing x. Since the Néel temperature of pure $BiFeO_3$ related to some rearrangements of the cycloidal spins in the systems is of ~643 K

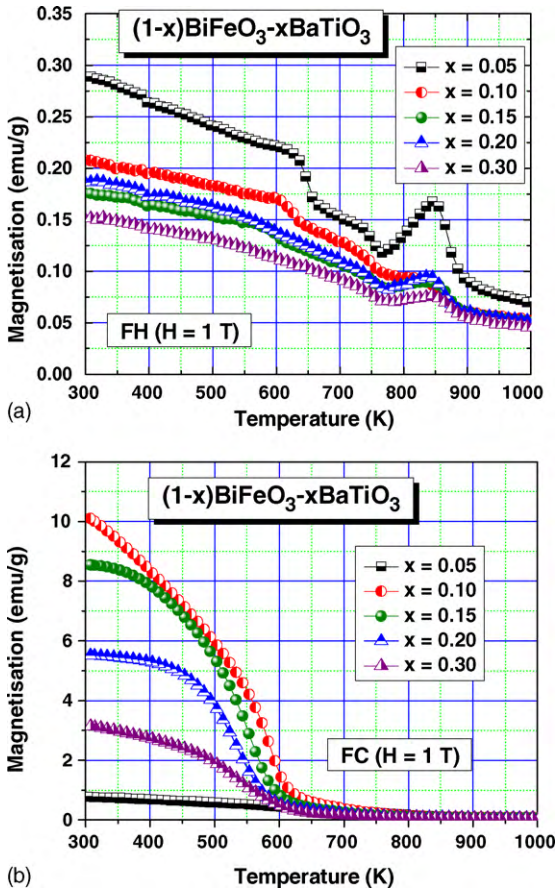

Fig. 6. Thermomagnetic data $M(T)$ of the $(1-x)BiFeO_3$–$xBaTiO_3$ ceramics at $H = 1$ T during: (a) field heating (FH) process; (b) field cooling (FC) process.

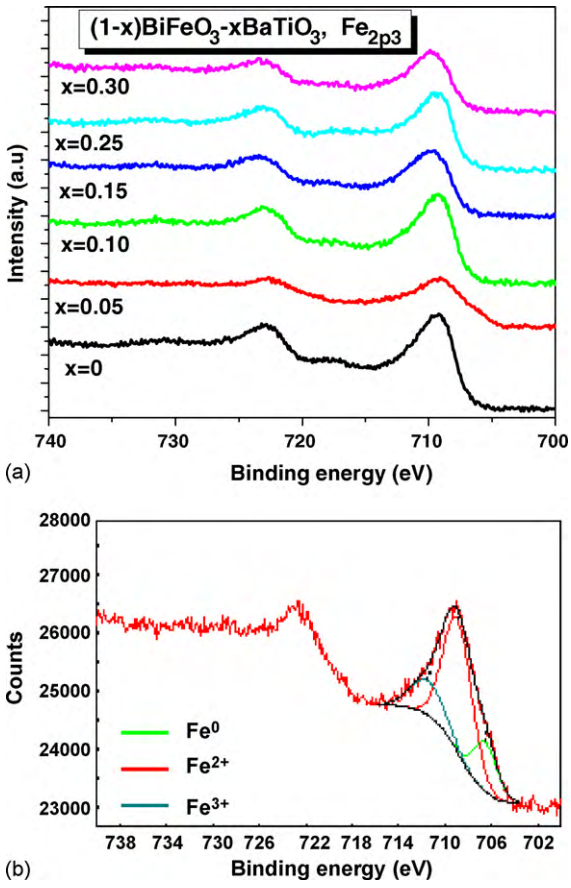

Fig. 7. (a) XPS spectra of $(1-x)BiFeO_3$–$xBaTiO_3$ $(0 \le x \le 0.30)$ ceramics; (b) fitting the XPS pectra for the composition $x = 0.05$.

[4–8], it seems that the increasing addition of $BaTiO_3$ produces a monotonous reduction of the Néel temperature. At FC cycle this anomaly completely disappears, due to the role of the magnetic driving force ($H = 1$ T), which induces a spin re-orientation, resulting in much higher values of the field-induced magnetization (Fig. 6(b)). Another important observation is that the FH/FC cycle causes changes of the magnetization by different amounts for each composition. A significant increase of magnetization for $x = 0.10$ (of about 50 times) is found, whereas for $x = 0.05$ an increase of around 3.5 times only is observed, by comparison with the values for the as-prepared ceramics. This means that the thermomagnetic FH/FC cycle acts not only in producing spin re-arrangements, but also induces irreversible compositional changes due to the $BiFeO_3$ chemical instability at high temperatures and variations of the oxygen stoichiometry associated with Fe^{3+}/Fe^{2+} transitions.

In order to better understand the composition-dependent magnetic properties related to the expected Fe^{2+}/Fe^{3+} ratio fluctuations in the solid solutions, a detailed X-ray Photoelectron Spectroscopy (XPS) analysis was performed on the surfaces and on the fractured sintered bodies. No differences were observed between the two types of experiments. Chemical microanalysis allowed to determine the cationic stoichiometry for each composition. XPS depth profiling revealed that all the species (Fig. 7(a and b)) are homogeneously distributed throughout the ceramic depth and also at the surface. The peak around 709 eV and two satellite peaks at ~718 and ~724.4 eV correspond to a combination of Fe^{2+}/Fe^{3+} states for all compositions (Fig. 7(a)). In addition, for $x = 0.05$ (Fig. 7(b)), beside the Fe^{2+}/Fe^{3+} states, also a small amount of metallic Fe^0 was found, most probably causing the high magnetization observed for this composition in the as-sintered ceramics. The presence of Fe^0 cannot be explained by using the available data and further experiments have to be performed in order to understand its origin. The effective magnetic moment to each state of the Fe ion in a bulk environment is determined by multiple factors, including the magnetic symmetry unit cell, super-exchange interaction mechanisms, magnetocrystalline anisotropy, etc. Calculations performed by using density-functional theory modeling for free Fe ions [41] gave values of $\sim 2.2\mu_B$ for Fe^0, and of $\sim 4.9\mu_B$ for Fe^{2+}, both lower than the values reported for Fe^{3+} of $\sim 5.9\mu_B$ [42]. If computing the average magnetic moment for the composition $x = 0.05$ as resulting from a mixture of free Fe ions, lower magnetization values would result than for the case of Fe^{3+} contributions only. However, the significant amount of Fe ions in reduced states for this sample is accompanied by an increased oxygen non-stoichiometry. Due to this effect, an enhancement of the double exchange Fe^{2+}–O–Fe^{3+} interactions between 2+ and 3+ Fe ions through the oxygen anion takes place, contributing to the rise of the ferromagnetic contribution in this sample, according to the calculations proposed in the Ref. [43]. After the FH/FC thermal excursion to high temperatures, the magnetization corresponding to the concentration $x = 0.05$ turned down to lower values, as showed in Fig. 6(b), because the re-oxidation of Fe^0 and reducing the level of oxygen vacancies led to a reduction of the double exchange contribution to the macroscopic magnetisation.

It results that the magnetic order in $BiFeO_3$ can be easily driven by proper magnetic or thermal history as well as by doping with $BaTiO_3$ compound and this might be a suitable strategy to induce a macroscopic magnetization in the view of obtaining multiferroic character at room temperature.

The mechanism of driving ferromagnetic properties in $BiFeO_3$-based ceramics by adding non-magnetic dopants or by forming

solid solutions is still under debate and research in various systems are currently reporting new data. In the present case, by some uncontrolled mechanism during the processing, the as-sintered composition $x = 0.05$ showed a higher magnetization, but this property looks as being rather accidental, than reproducible. In any case, it seems agreed that higher magnetization is found for small $BaTiO_3$ additions to $BiFeO_3$. A new series of samples around the compositions in the range $x = 0.05$–0.1 will be further produced in order to clarify the observed magnetic properties.

4. Conclusions

The complex impedance and magnetic properties of the $(1-x)BiFeO_3$–$xBaTiO_3$ ($0 \le x \le 0.30$) ceramics prepared by mixed oxides following a two-step sintering strategy were investigated. Pure single-phase perovskite phase was obtained for all the solid solutions of $(1-x)BiFeO_3$–$xBaTiO_3$, in the limit of XRD accuracy. By comparison with the single-step sintering method, a higher electrical homogeneity of the ceramic bodies resulted in better dielectric properties, with a single-component impedance plot and small losses ($\tan\delta < 3\%$) at room temperature. The magnetic data shown a typical antiferromagnetism in $BiFeO_3$ ceramics which can be turned into a ferrimagnetism by a FH/FC sequence under $H = 10$ kOe. A composition-dependent weak ferromagnetism with a maximum magnetization and coercive field for the composition $x = 0.05$ was determined. The thermomagnetic data indicate that magnetic properties are strongly composition and history-dependent and also that field cooling causes field-induced weak ferromagnetism in all compositions with a maximum magnetization for $x = 0.10$.

Low substitutions into A and B sites of the perovskite unit cell ABO_3 might represent a strategy in inducing ferromagnetism at room temperature in $BiFeO_3$ ceramics in order to produce a linear magnetoelectric effect, which is not compatible with the perfect antiferromagnetic spin order.

Acknowledgement

The financial support of the CNCSIS-PCCEID_76 grant is acknowledged.

References

[1] Y.H. Chu, L.W. Martin, M.B. Holcomb, R. Ramesh, Mater. Today 10 (2007) 16–23.
[2] S.M. Selbach, T. Tybell, M.A. Einarsrud, T. Grande, Adv. Mater. 20 (2008) 3692–3696.
[3] G. Catalan, J.F. Scott, Physics, Adv. Mater. 21 (2009) 2463–2485.
[4] F. Kubel, H. Schimid, Acta Crystallogr. B. 46 (1990) 698–702.
[5] P. Fischer, M. Polomska, I. Sosnowska, M. Szymanski, J. Phys. Solid State Phys. 13 (1980) 1931–1940.
[6] C. Ederer, N.A. Spaldin, Phys. Rev. B 71 (2005) 060401.
[7] J.B. Neaton, C. Ederer, U.V. Waghmare, N.A. Spaldin, K.M. Rabe, Phys. Rev. B71 (2005) 014113.
[8] D. Ricinschi, K.Y. Yun, M. Okuyama, J. Phys.: Condens. Matter. 18 (2006) L97–L105.
[9] J.R. Teague, R. Gerson, W.J. James, Solid State Commun. 8 (1970) 1073–1074.
[10] J. Li, J. Wang, M. Wuttig, R. Ramesh, N. Wang, B. Ruette, A.P. Pyatakov, A.K. Zvezdin, D. Viehland, Phys. Lett. 84 (2004) 5261–5263.
[11] K.Y. Yun, M. Noda, M. Okuyama, Appl. Phys. Lett. 83 (2003) 3981–3983.
[12] D. Lebeugle, D. Colson, A. Forget, M. Viret, Appl. Phys. Lett. 91 (2007) 022907.
[13] G.L. Yuan, S.W. Or, Y.P. Wang, Z.G. Liu, J.M. Liu, Solid State Commun. 138 (2006) 76–81.
[14] M.M. Kumar, V.R. Palkar, K. Srinivas, S.V. Suryanarayana, Appl. Phys. Lett. 76 (2000) 2764–2766.
[15] M.T. Buscaglia, L. Mitoseriu, V. Buscaglia, I. Pallecchi, M. Viviani, P. Nanni, A.S. Siri, J. Eur. Ceram. Soc. 26 (2006) 3027–3030.
[16] G.D. Achenbach, W.J. James, R. Gerson, J. Am. Ceram. Soc. 50 (1967) 437–1437.
[17] I. Sosnowska, T. Peterlin-Neumaier, E. Steichele, J. Phys. C: Solid State Phys. 15 (1982) 4835–4846.
[18] F. Chen, Q.F. Zhang, J.H. Li, Y.J. Qi, C.J. Lu, X.B. Chen, X.M. Ren, Y. Zhao, Appl. Phys. Lett. 89 (2006) 092910.
[19] V. Fruth, L. Mitoseriu, D. Berger, A. Ianculescu, C. Matei, S. Preda, M. Zaharescu, Prog. Solid State Chem. 35 (2007) 193–202.
[20] S.M. Selbach, M.A. Einarsrud, T. Tybell, T. Grande, J. Am. Ceram. Soc. 90 (2007) 3430–3434.
[21] A. Ianculescu, L. Mitoseriu, H. Chiriac, M.M. Carnasciali, A. Braileanu, R. Trusca, J. Optoel. Adv. Mater. 10 (2008) 1805–1809.
[22] M.M. Kumar, A. Srinivas, S.V. Suryanarayana, J. Appl. Phys. 87 (2000) 855–862.
[23] W.M. Zhu, Z.G. Ye, Ceram. Int. 30 (2004) 1435–1442.
[24] N. Wang, J. Cheng, A. Pyatakov, A.K. Zvezdin, J.F. Li, L.E. Cross, D. Viehland, Phys. Rev. B 72 (2005) 104434.
[25] F. Chang, N. Zhang, F. Yang, S. Wang, G. Song, J. Phys. D: Appl. Phys. 40 (2007) 7799–7803.
[26] V.A. Khomchenko, D.A. Kiselev, J.M. Vieira, L. Jian, A.L. Kholkin, A.M.L. Lopes, Y.G. Pogorelov, J.P. Araujo, M. Maglione, J. Appl. Phys. 103 (2008) 024105.
[27] M. Kumar, K.L. Yadav, Appl. Phys. Lett. 91 (2007) 112911.
[28] B. Kundys, A. Maignan, C. Martin, N. Nguyen, C. Simon, Appl. Phys. Lett. 92 (2008) 112905.
[29] F. Prihor, P. Postolache, L. Curecheriu, A. Ianculescu, L. Mitoseriu, Ferroelectrics 391 (2009) 76–82.
[30] J.R. Macdonald, Impedance Spectroscopy, Wiley, New York, 1987.
[31] M.K. Singh, R.S. Katiyar, J.F. Scott, J. Phys.: Condens. Matter 20 (2008) 252203.
[32] J.F. Scott, M.K. Singh, R.S. Katiyar, J. Phys. : Condens. Matter 20 (2008) 322203.
[33] Y.F. Popov, A.M. Kadomtseva, G.P. Vorobev, A.K. Zvezdin, Ferroelectrics 162 (1994) 135–140.
[34] Y.-Y. Li, Phys. Rev. 101 (1956) 1450.
[35] K.Y. Yun, M. Noda, M. Okuyama, H. Seki, H. Tabata, K. Saito, J. Appl. Phys. 96 (2004) 3399.
[36] A.E. Berkowitz, W.J. Schuele, P.J. Flanders, J. Appl. Phys. 39 (1968) 1261.
[37] S.H. Lim, M. Murakami, W.L. Sarney, S.Q. Ren, A. Varatharajan, V. Nagarajan, S. Fujino, M. Wuttig, I. Takeuchi, L.G. Salamanca-Riba, The effects of multiphase formation on strain relaxation and magnetization in multiferroic $BiFeO_3$ thin films, Thin Films, Adv. Mater., Adv. Funct. Mater. 17 (2007) 2594–2599.
[38] H. Béa, M. Bibes, S. Fusil, K. Bouzehouane, E. Jacquet, K. Rode, P. Bencok, A. Barthélémy, Phys. Rev. B 74 (2006), 020101(R).
[39] X.J. Lou, C.X. Yang, T.A. Tang, Y.Y. Lin, M. Zhang, J.F. Scott, Appl. Phys. Lett. 90 (2007) 262908.
[40] N. Itoh, T. Shimura, W. Sakamoto, T. Yogo, Ferroelectrics 356 (2007) 19–23.
[41] F. Starrost, H. Kim, S.C. Watson, E. Kaxiras, E.A. Carter, Phys. Rev. B 64 (2001) 235105.
[42] R. Tilley, Understanding Solids. The Science of Materials, Wiley & Sons Ltd., 2004, p. 370.
[43] N.A. Spaldin, W.E. Pickett, J. Solid State Chem. 176 (2003) 615–632.